Polymer Chemistry

ROYAL SOCIETY OF CHEMISTRY

PAPER

View Article Online
View Journal | View Issue

Cite this: *Polym. Chem.*, 2026, **17**, 1475

Lignin-based non-isocyanate polyurethanes by transurethanisation: catalyst selection towards covalent adaptable networks

Aline Rebejac,[a,b] Nathan Wybo,[a] Luc Avérous *[a] and Antoine Duval *[a,b]

This work reports the synthesis of lignin-based non-isocyanate polyurethanes (NIPUs) *via* transurethanisation (TU), aiming to develop biobased and recyclable covalent adaptable networks (CANs). A kinetic study of a model TU reaction enabled the selection of four catalysts for the preparation of crosslinked NIPUs from a Kraft lignin-derived polyol and hexamethylene dicarbamate. All these aromatic materials exhibited dynamic covalent behavior, allowing stress relaxation and efficient recycling through multiple thermo-mechanical cycles. The catalyst choice significantly influenced network architecture, mechanical performance, and recyclability. Iron and bismuth/zinc catalysts emerged as promising non-toxic alternatives to conventional tin-based catalysts, promoting efficient TU while limiting side reactions such as urea formation, which otherwise can compromise reprocessability. Chemical recycling was also demonstrated as a potential option for end-of-life valorization. Indeed, TU emerges as a robust and versatile framework for the synthesis of biobased and circular NIPUs. This approach clearly emphasizes how strategic catalyst selection is fundamental to tailoring material properties and ensuring recyclability.

Received 16th January 2026,
Accepted 9th March 2026

DOI: 10.1039/d6py00044d

rsc.li/polymers

Introduction

Polyurethanes (PUs) are a major class of polymer materials, with a global market estimated at 22 Mt in 2023, representing over 5% of the annual worldwide plastic production.[1] Thanks to the diversity of available building blocks, a wide array of macromolecular architectures can be achieved, leading to versatile properties and a broad range of applications, such as rigid or flexible foams, coatings, adhesives or elastomers. PUs are conventionally obtained by polyaddition between polyisocyanates and polyols, both of which are mostly fossil-based. For several decades, many efforts have been devoted to the development of biobased polyols for PUs.[2–4] Among the various biobased feedstocks, lignins are particularly well suited, thanks to their high content of OH groups, high functionality, and aromaticity (Fig. 1a), which contribute to improving the final materials' performance, such as mechanical and thermal properties. Besides, lignins are widely available from non-edible biomass, such as wood or agricultural residues. They are especially obtained as by-products of paper pulp production, mostly in the Kraft process. Around 70 Mt per year of Kraft lignin (KL) are extracted from woody biomass in pulp mills,[5,6] and 5 to 20% could be isolated without compromising the energy production coming from its combustion in recovery boilers in Kraft pulp mills.[7,8] This potentially represents available amounts of over 10 Mt per year, although the actual industrial production is still far from these figures.[8,9]

The use of lignins in PUs has been thoroughly studied.[10–14] However, the development of biobased polyols does not solve another important issue of PU production, which is the use of isocyanates. Isocyanates are toxic and sensitizing compounds,[15,16] strongly regulated in Europe by REACH, and synthesized from highly toxic phosgene. Different chemical strategies have thus been developed to produce non-isocyanate PUs (NIPUs).[17] The reaction between cyclic carbonates and amines, leading to polyhydroxyurethanes (PHUs), has been the most studied. Recent developments allowed promising improvements for applications of PHUs in, *e.g.*, adhesives, coatings or foams.[18–21] Lignin has already been successfully used in PHU synthesis, after chemical modifications to introduce amine[22–25] or cyclic carbonate groups[26–32] into its structure.

Beyond aminolysis, another strategy to synthesize NIPUs relies on the transurethanisation (TU) reaction between polyols and polycarbamates, which can be easily obtained from polyamines and dimethyl carbonate (Scheme 1). Unlike PHUs, this approach has the advantage of yielding NIPUs with chemical structures similar to those of conventional PUs, without the generation of an additional OH group. It can also benefit from

[a]*BioTeam/ICPEES-ECPM, UMR CNRS 7515, Université de Strasbourg, 25 rue Becquerel, 67087 Strasbourg Cedex 2, France. E-mail: luc.averous@unistra.fr, antoine.duval@unistra.fr*
[b]*Soprema, 15 rue de Saint Nazaire, 67100 Strasbourg, France*

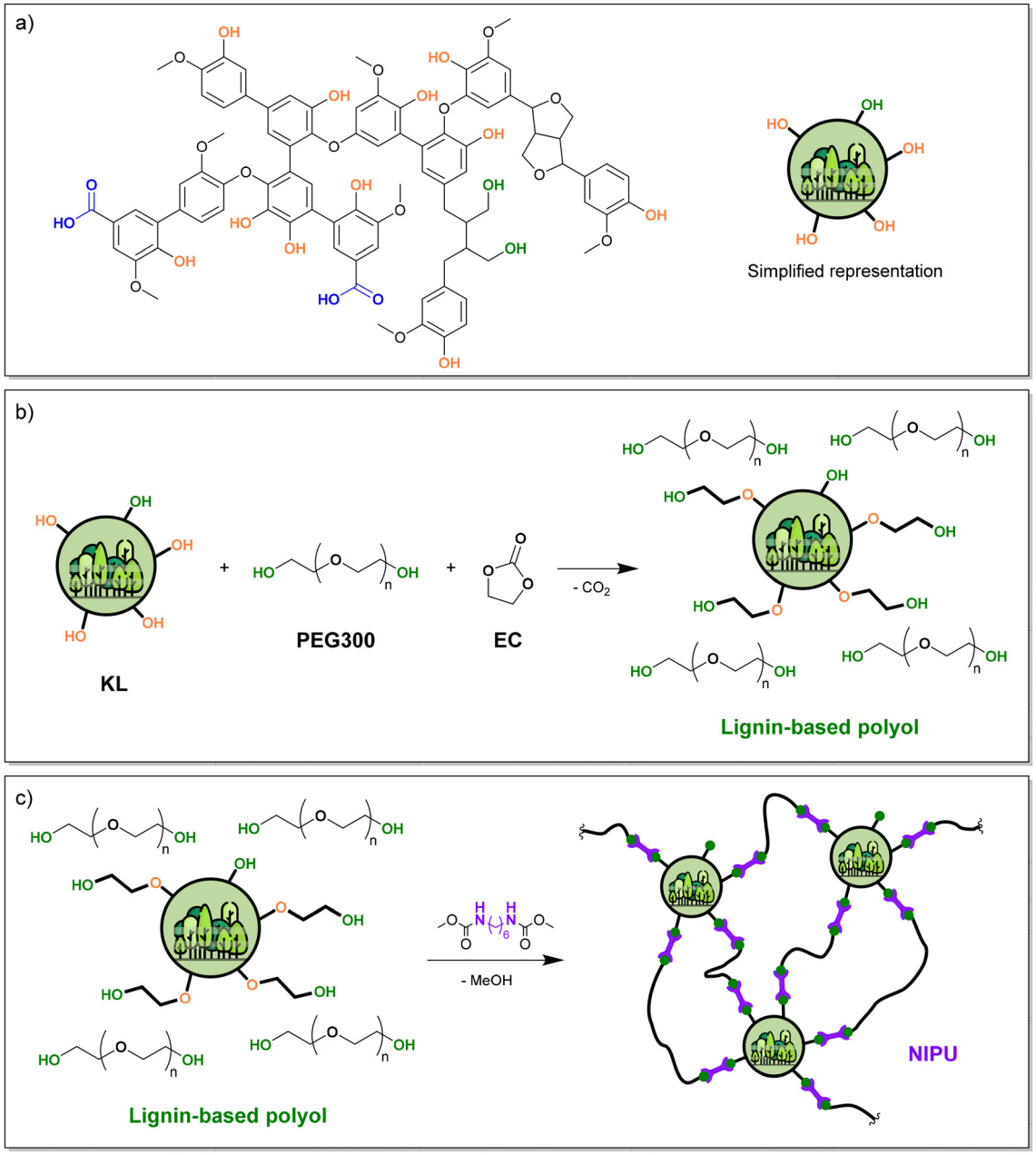

Fig. 1 (a) Representative structure of KL, (b) scheme of lignin-based polyol synthesis with EC and (c) scheme of NIPU synthesis from lignin-based polyol and HMDC.

the last decades of research on biobased polyols for PUs, since they can be directly employed to produce NIPUs by TU. The synthesis of NIPUs by TU has mostly been applied to thermoplastics[33–39] or to oligomeric linear precursors for crosslinked hybrid networks.[40–44] Recent studies have shown that high molar masses can be achieved,[45,46] despite side reactions leading to the formation of urea and carbonate linkages in the NIPU backbone.

Our group recently showed that the TU reaction could also be applied to synthesise crosslinked, aromatic and biobased NIPUs from lignins.[47] Lignin was first converted into a liquid polyol containing only primary aliphatic OH groups (Fig. 1b),[48] and reacted with hexamethylene dicarbamate (HMDC) to prepare NIPUs (Fig. 1c), whose properties can be tailored by adjusting the lignin content. When the materials were synthesized with an excess of OH with respect to carbamates, free OH groups present in the network could generate bond exchange by TU, conferring a Covalent Adaptable Network (CAN) behaviour to the materials. CANs bridge the gap between permanent networks and reprocessability, offering high mechanical performance alongside self-healing and circularity. By leveraging dynamic covalent chemistry, they allow

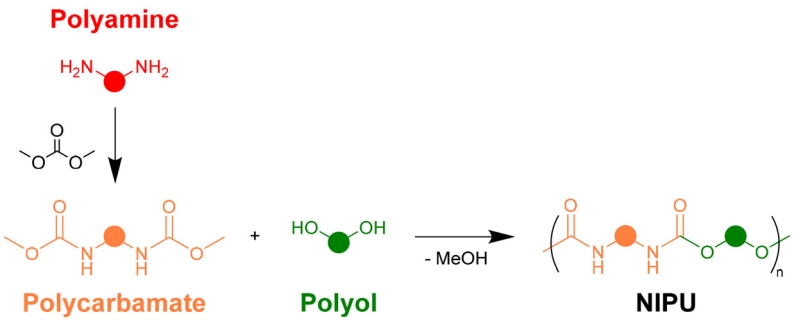

Scheme 1 Synthesis of NIPUs by transurethanisation (TU).

for multiple reprocessing cycles and structural reconfiguration without losing the crosslinking.

However, this previous work showed that the reprocessability of the materials was limited,[47] probably because of the use of 1,5,7-triazabicyclo[4.4.0]dec-5-ene (TBD) as a catalyst. Indeed, TBD can promote side reactions leading to the formation of permanent urea or allophanate linkages,[49] and it degrades at temperatures above 160 °C,[50] leading to a rapid loss of catalytic activity. In this work, we aimed at overcoming these limitations and enhancing the material properties and recyclability thanks to catalyst selection. A thorough evaluation of the impact of different catalysts on the synthesis, properties and recyclability of lignin-based NIPUs produced by TU was performed. A kinetic study of a model TU reaction was used to select 4 catalysts, which were then employed to synthesize NIPUs with HMDC and a polyol prepared from KL (Fig. 1c). The materials were deeply characterized. The recycling potential of these different lignin-based NIPUs was estimated through multiple cycles to highlight the potential of the TU reaction for the safe synthesis of biobased and recyclable NIPU-based CANs.

Experimental section

Materials

Softwood Kraft lignin (Lineo®, KL) was kindly provided by Stora Enso. It was dried in a vacuum oven at 40 °C overnight prior to use. Dimethylcarbonate (DMC, 99%) and ethylene carbonate (EC, 99%) were purchased from Alfa Aesar. Hexamethylenediamine (HMDA) was purchased from BASF. Polyethylene glycol with M_n = 300 g mol^{-1} (PEG300) was purchased from Acros Organics. Polyethylene glycol monomethyl ether with M_n = 500 g mol^{-1} (PEG500MM) was provided by Fluka Analytical. Potassium carbonate (K_2CO_3, >99%) and sodium hydroxide (NaOH, ≥97%) were bought from Fischer Scientific and VWR, respectively. Zirconium(IV) acetylacetonate (97%), iron(III) acetylacetonate (97%), dibutyltin dilaurate (95%), chromium(III) acetylacetonate (97%), and triazabicyclo [4.4.0]dec-5-ene (TBD, 98%) were purchased from Sigma-Aldrich. Bis-(dodecylthio)dioctylstannane (Niax LC5612) and bismuth/zinc octanoate blend (Reaxis C717) were supplied by Momentive and Reaxis, respectively. Deuterated chloroform ($CDCl_3$, 99.8%) was purchased from Eurisotop.

Synthesis of hexamethylene dicarbamate (HMDC)

HMDA (50 g, 430 mmol, 1 eq.), DMC (388 g, 4.3 mol, 10 eq.), and TBD (6 g, 43 mmol, 0.1 eq.) were stirred under argon at 90 °C for 14 h. The reaction mixture was then cooled down to room temperature and placed in an ice bath for 2 h, resulting in the precipitation of the product. The precipitate was recovered by filtration, rinsed with water, and dried under vacuum overnight. HMDC was obtained as a white powder with an average yield of 92% (2 replicates).

^{1}H NMR (400 MHz, $CDCl_3$): δ (ppm) 4.69 (br, 2H, NH), 3.64 (s, 6H, CH_3, d), 3.14 (m, 4H, CH_2), 1.47 (m, 4H, CH_2), 1.31 (m, 4H, CH_2).

Kinetic study of the model TU reaction

HMDC (1 g, 4.3 mmol, 1 eq.), PEG500MM (4.3 g, 8.6 mmol, 2 eq.), and the catalyst (0.9 mmol, 0.2 eq.) were stirred in a round-bottom flask under argon at 140 °C for 24 h. Aliquots were taken every hour from 0 to 6 h and at 24 h and analysed by ^{1}H NMR in $CDCl_3$. The yield of the urethane product was calculated by comparing the integrations of the peaks at 4.16 ppm (–C$\underline{H}_2$–O–C(O)– in the newly formed urethane product) and 3.12 ppm (–C$\underline{H}_2$–NH–C(O)– in HMDC and in the newly formed urethane product).

Synthesis of lignin-based polyol

Lignin-based polyol was synthesized according to a known procedure.[48] PEG300, KL and EC were dried overnight at 40 °C under vacuum. KL (80 g, 6.33 mmol g^{-1} of reactive groups, *i.e.* the sum of OH + COOH), PEG300 (120 g), EC (49 g, 0.56 mol, 1.1 eq. with respect to the reactive groups in KL), and NaOH (5.3 g, 0.13 mol, 0.25 eq. with respect to the reactive groups in KL) were placed in a round-bottom flask under mechanical agitation and reacted at 130 °C for 4 h under argon. The brown liquid lignin-based polyol obtained at the end of the reaction was used without further purification. The conversion of phenol groups was 100%, and the final OH content of the polyol was 7.22 mmol g^{-1}, as measured by ^{31}P NMR.

NIPU synthesis

Polyol (10 g, 72.2 mmol of OH, 1 eq.), HMDC (7.55 g, 32.5 mmol, 0.45 eq.) and the catalyst (0.05 eq.) were stirred mechanically in a round-bottom flask at 120 °C under argon until a homogeneous mixture was obtained. The mixture was then poured into a PTFE plate and incubated in an oven under an argon flux at 140 °C for 3 h, then at 160 °C for 1.5 h, and finally at 160 °C under vacuum for 30 min. The obtained material was then pressed into a sheet (100 mm × 100 mm × 1 mm) by compression molding (30 min at 160 °C under 150 bar) using a hydraulic press (Lab Tech Engineering Company Ltd).

NIPU recycling

Dry NIPU sheets were finely ground in a small grinder. For thermomechanical recycling, the powder was directly thermo-compressed into a sheet under conditions similar to those of NIPU synthesis (30 min at 160 °C under 150 bar). For chemical recycling, 10 g of material and 100 mL of methanol were introduced into a 300 mL Parr reactor. The reactor was flushed with argon before being sealed and heated at 140 °C under agitation for 24 h, reaching a maximum pressure of about 10 bar. After cooling down to room temperature, the brown homogeneous liquid obtained was then evaporated under vacuum at 40 °C, yielding the depolymerized mixture. The mixture was then cured, as in the case of the initial NIPU synthesis, to obtain the chemically recycled material.

Characterization studies

^{1}H and ^{31}P NMR spectra were recorded on a Bruker 400 MHz spectrometer at 25 °C. For ^{1}H NMR, 16 scans were recorded. ^{31}P NMR of lignin was performed according to the standard protocol.[51] 128 scans were acquired with a 15 s relaxation delay.

Fourier transform infrared (FTIR) spectra were acquired with a Nicolet 380 spectrometer from Thermo Scientific, equipped with an attenuated total reflectance (ATR) diamond module. 32 scans were recorded in the range of 4000–500 cm^{-1}.

Differential scanning calorimetry (DSC) was performed on a DSC 25 Discovery series (TA Instruments). Samples were first equilibrated at 105 °C for 10 min, then cooled down to −60 °C at 10 °C min^{-1} and finally heated to 200 °C at 10 °C min^{-1}. T_g was recorded as the change in slope during the second heating run.

Thermogravimetric analyses (TGAs) were performed on a TGA 2 STAR System (Mettler Toledo). Samples were heated from 45 to 700 °C at 20 °C min^{-1} under N_2 or air flow (25 mL min^{-1}).

The swelling ratio (SR) and gel fraction (GF) were determined by immersion of dry samples of initial mass m_i in acetone or water for 48 h. After measuring the mass of the swollen samples (m_1), they were dried in a vacuum oven for 24 h at 50 °C, and their final mass m_f was measured. The test was performed in triplicate, and average values and standard deviations are reported. SR and GF were calculated using eqn (1) and (2), respectively:

$$\mathrm{SR}\,(\%) = \frac{m_1 - m_f}{m_f} \times 100 \quad (1)$$

$$\mathrm{GF}\,(\%) = \frac{m_f}{m_i} \times 100 \quad (2)$$

Dynamic mechanical analysis (DMA) and stress relaxation experiments were performed on a Discovery HR-3 hybrid rheometer (TA Instruments). For DMA, rectangular samples (approximately 20 mm × 10 mm × 1 mm) were tested in torsion mode (0.01% strain, 1 Hz), from −50 to 150 °C (3 °C min^{-1} ramp). T_α was determined at the maximum of the tan δ curves. For stress relaxation, sample discs (25 mm diameter, 1 mm thickness) were tested using a 25 mm parallel plate geometry. A series of experiments at different temperatures (from 140 to 180 °C) were performed successively on the same sample after equilibration for 20 min, with a fixed gap of around 1 mm and 1% strain.

Uniaxial tensile tests were performed at 23 °C using an Instron 68TM-10 universal testing system equipped with a 10 kN load cell, at a constant crosshead speed of 20 mm min^{-1}, following the ISO 527 standard. 5 dumbbell-shaped samples (45 mm × 5 mm × 1 mm) were cut from the films and tested until failure. Young's modulus (E), stress at break (σ) and elongation at break (ε) are reported as average values with standard deviations.

Results and discussion

Screening of catalysts for transurethanisation

In our previous work, TBD was used to catalyse the NIPU synthesis by TU,[47] but it proved to be inadequate for enabling reprocessability. Alternative catalysts able to promote the carbamate exchange reaction were thus screened (Table 1). Tin-based catalysts, especially dibutyltin dilaurate (DBTDL, **Sn-A**), are routinely used in conventional PU synthesis and have also been shown to be active for catalysing bond exchange in crosslinked PUs.[52–56] Other tin-based catalysts have been developed

Table 1 Urethane yield after 24 h and the reaction rate constant of the TU reaction with different catalysts

Acronym	Chemical name	Urethane yield after 24 h (%)	k (10^{-5} L mol^{-1} s^{-1})
Fe	Iron(III) acetylacetonate	84	6.06 ± 0.31
Sn-A	Dibutyltin dilaurate	83	4.95 ± 0.22
TBD	Triazabicyclo[4.4.0]dec-5-ene	72	4.25 ± 0.62
Bi-Zn	Bismuth/zinc octanoate blend	72	2.23 ± 0.20
Zr	Zirconium(IV) acetylacetonate	54	1.51 ± 0.05
K_2CO_3	Potassium carbonate	62	1.01 ± 0.05
Sn-B	Bis-(dodecylthio)dioctylstannane	52	0.62 ± 0.04
NaOH	Sodium hydroxide	28	0.13 ± 0.02

as alternatives to DBTDL, such as bis-(dodecylthio)dioctylstannane (**Sn-B**), which was also investigated. However, their high toxicity makes it necessary to seek more sustainable alternatives.[57] Zirconium, bismuth and iron complexes have previously been described as potential alternatives to tin-based catalysts, either for the synthesis of PUs, for TU reactions, or to promote bond exchange in crosslinked PUs.[55,58–61] We then evaluated iron(III) acetylacetonate (**Fe**), zirconium(IV) acetylacetonate (**Zr**), and a commercial bismuth/zinc octanoate blend (**Bi-Zn**). Their chemical structures are shown in Fig. S1 in the SI. Since the lignin-based polyols used for the NIPU synthesis are not purified, they contain the basic catalyst employed in their synthesis. Therefore, we also evaluated the influence of K_2CO_3 and **NaOH** on the TU kinetics, since both can be used for the polyol synthesis.

A model TU reaction between PEG500MM and HMDC was performed at 140 °C. Urethane product yield was evaluated by ^{1}H NMR from 0 to 6 h (Fig. 2), with an extension to 24 h to reach thermodynamic equilibrium (Table 1). Yield was quantified through the integration of the characteristic signal of the newly formed urethanes at 4.13 ppm. The corresponding ^{1}H NMR spectra are available in the SI (Fig. S2–S9). The TU reaction was previously shown to be first order with respect to the carbamate and alcohol, *i.e.* overall second order.[58,62] Rate constants were calculated based on this assumption, as detailed in the SI (Fig. S10), and the results are provided in Table 1.

Highest yields are achieved with **Sn-A** and **Fe** (83–84%), followed by **TBD** and **Bi-Zn** (72%). These catalysts also gave the highest reaction rates. The difference between **Sn-A** and **Sn-B** clearly shows that the nature of the ligands also influences the catalytic activity, as previously reported.[55,59] Among the inorganic basic catalysts tested, K_2CO_3 shows significant activity to catalyse the TU reaction. Although the rate constant is low compared to most of the metal catalysts, it leads to a 62% yield of urethane product after 24 h. Indeed, it has been recently used as a catalyst for the synthesis of thermoplastic NIPUs by TU.[45] On the other hand, **NaOH** has practically no catalytic activity for the TU reaction, with a urethane yield below 5% after 6 h of reaction. Based on these results, 4 catalysts were selected for materials synthesis: **TBD**, **Sn-A**, **Fe** and **Bi-Zn**. **NaOH** is preferred for polyol synthesis, as it does not significantly catalyse the TU reaction and therefore does not influence the study of the TU catalysts.

Elaboration of lignin-based NIPUs by transurethanisation

A lignin-based polyol was synthesized following a reported methodology.[48] Lignin was reacted with EC in the presence of PEG, leading in a single step to a homogeneous, liquid polyol containing only primary aliphatic OH groups (Fig. 1b). The reaction mechanism is detailed in the SI (Scheme S1). The reaction is catalysed by bases, typically K_2CO_3 or TBD.[47,48,63] However, since the polyols are not purified, the corresponding catalyst remains present during the NIPU synthesis by TU. In this case, NaOH was chosen as the catalyst, since its impact on the TU reaction is moderate (Fig. 2), thus allowing for the evaluation of various catalysts for the NIPU synthesis by TU. The lignin content of the polyol was set to 40 wt% with respect to PEG. Full conversion of the phenolic OH groups of lignin into aliphatic OH was shown by ^{31}P NMR (Fig. S11 in the SI).

NIPU materials were then synthesized by TU between the lignin-based polyol and HMDC (Fig. 1c), as in our previous work,[47] but with some adjustments to the process to optimize material homogeneity and repeatability. The reactants were first homogenized at 120 °C, above the HMDC melting point, under mechanical stirring instead of manual mixing, and a final step under vacuum was added to drive curing to completion.

The carbamate to OH ratio was set to 0.9 : 1, ensuring the presence of free OH groups within the final networks. The 4 catalysts previously selected were employed, resulting in 4 materials to be compared: **NIPU-Sn**, **NIPU-TBD**, **NIPU-Fe** and **NIPU-Bi-Zn**. The chemical structures of the materials were evaluated by FTIR (Fig. 3). All the materials show a noticeable

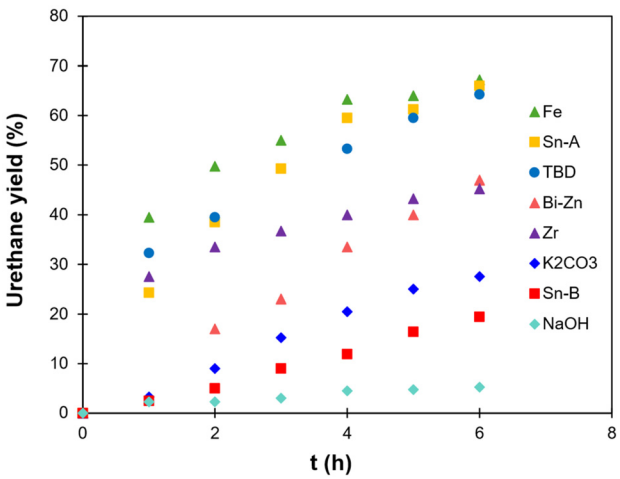

Fig. 2 Kinetic study at 140 °C of the model TU reaction by ^{1}H NMR: yield of urethane product depending on the catalyst used.

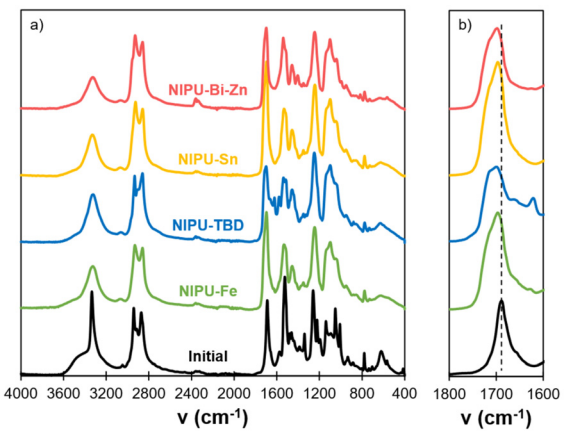

Fig. 3 (a) FTIR spectra of the initial reactant mixture before polymerization and the resulting NIPU materials prepared with various catalysts. (b) Details of the C=O stretching region.

decrease of the O–H stretching band of the polyol (3480 cm^{-1}), along with an enlargement of the N–H stretching band of urethanes (3335 cm^{-1}), indicative of the successful TU reaction. Noticeable differences are evidenced in the C═O stretching region (1600–1800 cm^{-1}, Fig. 3b). For all materials, the C═O stretching band of HMDC at 1690 cm^{-1} is shifted towards higher wavenumbers, confirming its full consumption during the TU reaction. **NIPU-TBD** presents two bands at 1662 cm^{-1} and 1625 cm^{-1}, which are not visible for the other materials. They can be assigned to the C═O stretching in free and H-bonded ureas and may also contain contributions from allophanate and biuret structures, which are formed by side reactions during TU. Interestingly, it seems that **Sn-A**, **Fe** and **Bi-Zn** catalysts can limit such side reactions during the NIPU synthesis by TU. The large C═O stretching bands may result from the different configurations of urethane bonds (free or hydrogen-bonded), as discussed later, and from contributions of the carboxylate or acetylacetonate ligands of the catalysts (Fig. S1).

Influence of the catalyst nature on NIPU properties

Swelling ratios (SR) and gel fractions (GF) were measured in water and acetone, which show diverse affinities for the different constituents of the materials. PEG is highly soluble in water, whereas KL is more soluble in acetone. The results are provided in Table 2. GF values are quite high, from 80 to 87% in water and 72 to 89% in acetone, confirming the crosslinked nature of the materials. **NIPU-TBD** presents a higher GF in acetone than in water, while the opposite is found for the other materials. It also has the lowest SR in acetone, potentially indicating a higher crosslink density, although its SR in water is in the middle range. Urea linkages observed by FTIR potentially act as physical crosslinks *via* hydrogen bonding, leading to the low SR and high GF in acetone, but the hydrogen bonds can be disrupted in water, causing higher SR and lower GF.

As compared to NIPU materials prepared from hardwood organosolv lignin (OL) with a similar formulation in our previous work,[47] GF values are higher and the SR values are lower, indicating higher crosslinking. This can be related to the higher functionality of KL compared to the OL previously employed (6.33 mmol g^{-1} of Al-OH, Ph-OH and COOH in KL against 4.68 mmol g^{-1} in OL).

Thermal degradation of the materials was evaluated by TGA (Table 3 and Fig. S13 in the SI). All the materials present a high thermal stability, with $T_{5\%}$ above 230 °C under nitrogen or air. The main degradation temperature T_d is above 300 °C for all materials, in a temperature range commonly reported for both lignin[64–66] and PEG[38,67] main thermal degradations. The catalyst could potentially influence the degradation pathway, since **NIPU-Fe** presents a higher T_d than the other materials (346 °C against 304–317 °C), but further studies would be needed to understand the phenomenon. DSC analyses show that all the materials present a T_g below ambient temperature (Table 3 and Fig. 4a). **NIPU-TBD**, **NIPU-Sn**, and to a lesser extent **NIPU-Fe** present a second inflexion point close to 120 °C. This temperature is slightly lower than the T_g of KL (143 °C, Fig. S14 in the SI). It could thus be related to a second T_g, originating from separated domains with a high lignin content. **NIPU-Bi-Zn**, which does not present such phase separation, has a T_g higher than the other materials (−4 °C against −10 to −14 °C), probably because lignin is more present in the "soft" phase since lignin-rich domains are absent.

Thermomechanical properties were measured by DMA (Table 3, Fig. 4c and d, and Fig. S15 in the SI). All the NIPU materials present a broad glass transition, resulting in very large peaks of tan δ. This indicates a complex and heterogeneous network morphology, directly linked to the heterogeneity of KL. T_α values are close to room temperature for all materials but do not correlate well with the T_g values measured by DSC. The materials present a clear rubbery plateau, confirming their crosslinked nature. According to rubber elasticity theory, the crosslink density ν is usually calculated from the value of G' at T_α + 50 °C. However, given the broadness of the transition observed here, the rubbery plateau is clearly not reached at T_α + 50 °C. It is only reached at about 100 °C for **NIPU-Fe**, **NIPU-Sn** and **NIPU-Bi-Zn**, whereas **NIPU-TBD** shows a different behaviour, with a continuous decrease up to 150 °C, where the measurement was stopped. Therefore, values of G' on the rubbery plateau can only give a trend in the crosslink densities of the materials. **NIPU-Sn** has the lowest crosslink density, followed by **NIPU-Bi-Zn** and **NIPU-Fe**, confirming the trend of the SR in acetone. **NIPU-TBD** has a significantly higher G' than the other materials between 0 and 120 °C. It is probably related to the presence of urea bonds acting as physical crosslinks. The continuous decrease of G' with increasing temperature may be the consequence of the rupture of the physical bonds.

Mechanical properties were then evaluated by uniaxial tensile tests (Table 3, Fig. 4b and Fig. S16 in the SI).

Table 2 Swelling ratios (SR) and gel fractions (GF) of the NIPU materials in water and acetone

Material	SR H_2O (%)	SR acetone (%)	GF H_2O (%)	GF acetone (%)
NIPU-Fe	52 ± 1	42 ± 7	80 ± 1	72 ± 1
NIPU-TBD	41 ± 1	26 ± 1	83 ± 1	89 ± 1
NIPU-Sn	41 ± 3	53 ± 1	85 ± 2	75 ± 2
NIPU-Bi-Zn	31 ± 3	48 ± 1	87 ± 1	80 ± 2

Table 3 Main properties of the NIPU materials, as measured by TGA (under N_2), DSC, DMA and uniaxial tensile tests. For the mechanical properties, different capital letters indicate statistically significant differences (HSD Tukey test, α = 0.05)

Material	$T_{5\%}$ (°C)	T_d (°C)	T_g (°C)	T_α (°C)	E (MPa)	σ (MPa)	ε (%)
NIPU-Fe	235	346	−14	18	7 ± 1^{A}	1.7 ± 0.2^{A}	28 ± 3^{A}
NIPU-TBD	250	304	−13	20	32 ± 2^{B}	4.5 ± 0.4^{B}	27 ± 4^{A}
NIPU-Sn	241	317	−10	10	$10 \pm 1^{A,C}$	1.0 ± 0.3^{C}	26 ± 8^{A}
NIPU-Bi-Zn	251	312	−4	19	10 ± 1^{C}	4.2 ± 0.3^{B}	72 ± 2^{B}

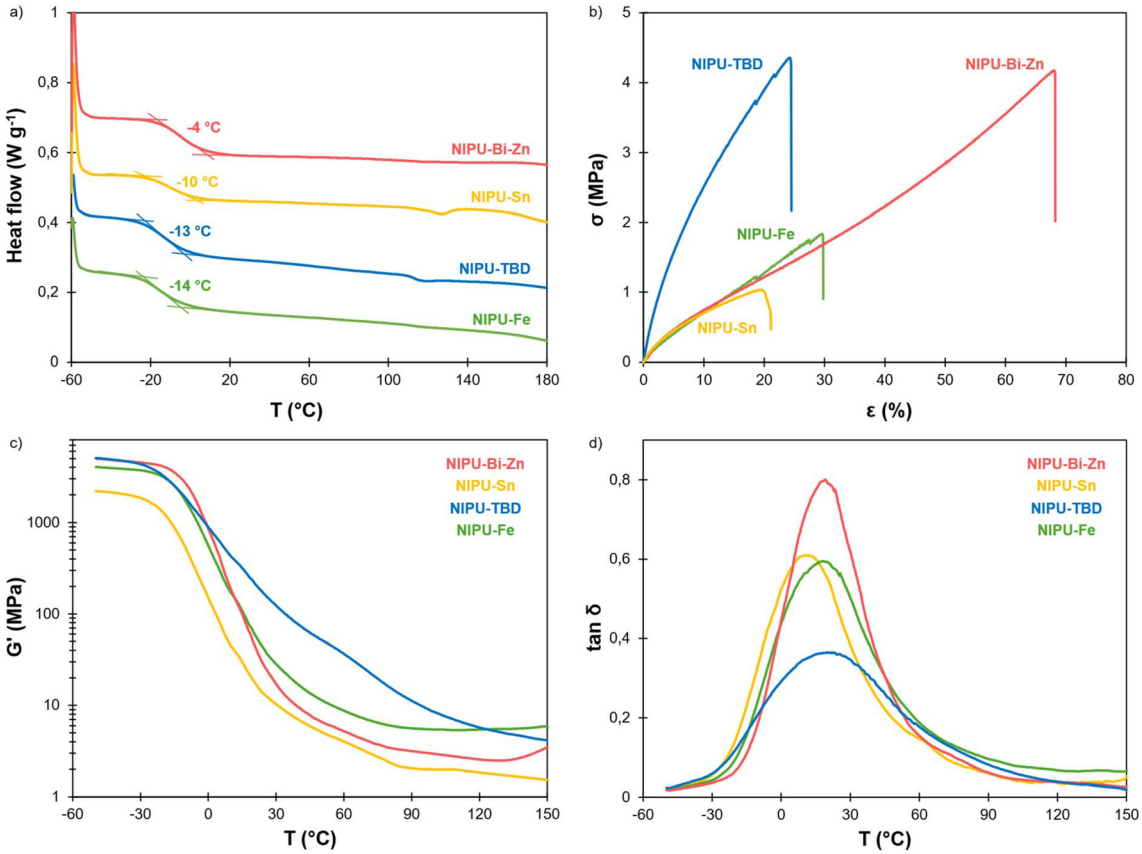

Fig. 4 Characterization of the NIPU materials by (a) DSC, (b) uniaxial tensile tests, (c) storage modulus G' and (d) tan δ measured by DMA.

Interestingly, significantly distinct behaviours were observed depending on the catalyst used for NIPU synthesis. **NIPU-Fe**, **NIPU-Sn** and **NIPU-Bi-Zn** present similar Young's modulus, in the range of 7 to 10 MPa. However, **NIPU-Bi-Zn** has a much higher elongation at break (72 ± 2%), leading to a higher tensile strength and to the highest toughness of the material series. It outperforms the mechanical properties of most lignin-based NIPU materials reported to date (Fig. S17).[23,24,27,30,32,47] Unlike other materials, a single T_g was detected by DSC for **NIPU-Bi-Zn**, indicating higher homogeneity and the formation of a single phase. The possible phase separation evidenced by DSC for **NIPU-Sn** could lead to defects that cause the early rupture of the material, explaining its lower tensile strength.

NIPU-TBD has a significantly different behaviour. It presents a much higher Young's modulus, more than 3 times the average value of the other materials, and a high tensile strength. It is the consequence of the presence of ureas, as evidenced by FTIR, which leads to more hydrogen bonds that contribute to enhancing the mechanical properties. Compared to a material synthesized in our previous study with a similar formulation but a different lignin,[47] this material has a higher Young's modulus (32 against 19 MPa) and a higher tensile strength (4.5 against 2.5 MPa). It means that the lignin type, *i.e.*, softwood KL *vs.* hardwood OL, has a significant impact on the material properties. Testing additional lignin types could help better understand and establish the "structure–properties" relationships.

Characterization of the dynamic behaviour

The NIPU materials were synthesized with a carbamate to OH ratio of 0.9 : 1, ensuring that free OH groups were present in the networks. Free OH groups can thus react by TU with the urethane bonds constituting the networks, conferring a dynamic covalent behaviour to the materials.[47] Stress relaxation measurements were performed to evaluate the impact of the catalyst on the bond exchange. All the NIPU materials showed complete stress relaxation between 140 and 180 °C (Fig. 5a and Fig. S18 in the SI). This shows that TU can be employed to synthesise NIPU CANs, thanks to an appropriate network design ensuring the presence of free OH groups within the networks.

The non-normalized relaxation curves are presented in the SI (Fig. S18). They were fitted with a stretched exponential model (Kohlrausch–Williams–Watts function), according to eqn (3):

$$G(t) = G_0 e^{-\left(\frac{t}{\tau^*}\right)^{\beta}} \quad (3)$$

where G_0 is the modulus extrapolated to $t = 0$, τ^* is the relaxation time and β is an exponent characterising the broadness of the distribution of relaxation times ($0 < \beta < 1$).

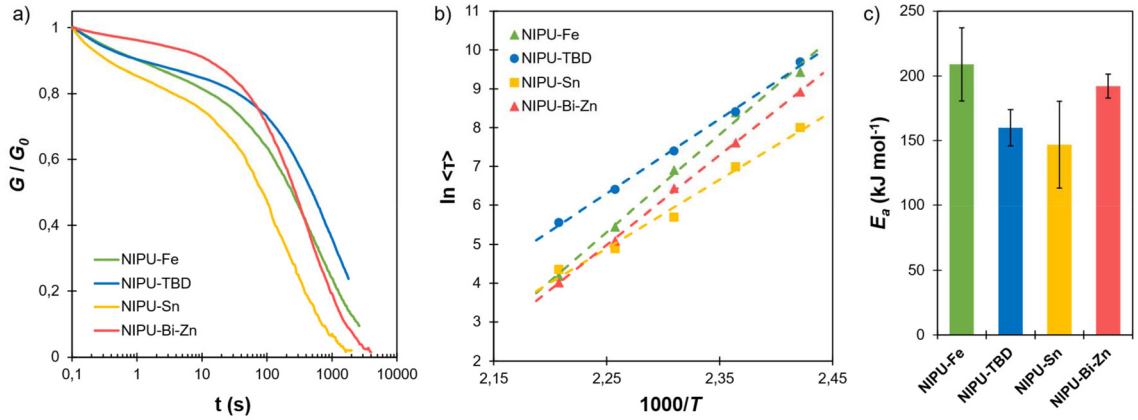

Fig. 5 Results of stress relaxation experiments of the NIPU materials: (a) normalized relaxation modulus measured at 160 °C, (b) Arrhenius plot of the average relaxation times $\langle\tau\rangle$ and (c) activation energies E_a of the bond exchange process.

The data were accurately fitted by this model for $t > 1$ s. Fast relaxation within the first second, which was especially pronounced for **NIPU-Fe** and **NIPU-Sn** (Fig. 5a and Fig. S18 in the SI), was not taken into consideration. The average relaxation $\langle\tau\rangle$ time was calculated according to eqn (4):

$$\langle\tau\rangle = \frac{\tau^{*}\Gamma\left(\frac{1}{\beta}\right)}{\beta} \quad (4)$$

where Γ is the gamma function.

For all the NIPU materials, $\langle\tau\rangle$ follows an Arrhenius law (Fig. 5b), from which the activation energy E_a could be evaluated (Fig. 5c). These results clearly show the impact of the catalyst on the relaxation properties. **NIPU-Sn** shows the fastest relaxation and **NIPU-TBD** the slowest, while **NIPU-Fe** and **NIPU-Bi-Zn** present intermediate behaviours (Fig. 5b). The catalyst efficiencies are different from the results of the model transurethanisation study (Table 1). At high temperature, the differences between catalysts vanish, and apart from **NIPU-TBD**, all the NIPU materials show similar relaxation times, with $\langle\tau\rangle$ close to 1 min at 180 °C (Fig. 5b and Tables S1–S4 in the SI), faster than many of the previously reported lignin-based vitrimers.[68–74]

The activation energy E_a was also found to be catalyst-dependent, with **Fe** and **Bi-Zn** leading to higher activation energy than **TBD** and **Sn** (Fig. 5c). E_a around 200 kJ mol^{-1} measured for **NIPU-Fe** is on the high end of values reported for vitrimers, a positive feature for achieving fast reprocessing at high temperature while maintaining high dimensional stability at usage temperature.

Two distinct mechanisms are known to allow bond exchange in crosslinked PUs (Scheme S2 in the SI).[75] Associative TU can take place in the presence of free OH groups, as in the present case. However, a dissociative pathway involving the cleavage of urethanes into isocyanates and alcohol can also take place, and both mechanisms probably coexist. The catalyst type is thought to influence the chemical pathway. Elizalde *et al.* reported that DBTDL seemed to promote dissociative exchange.[76] On the other hand, bismuth catalysts were shown to promote an associative mechanism, since isocyanates were not detected in the model study of Jousseaume *et al.*[58] For all the NIPU materials studied here, G_0 increases with the temperature (Fig. S18 and Tables S1–S4 in the SI), as predicted by rubber elasticity theory for CAN following an associative bond exchange, *i.e.* vitrimers.[71,77–79] These results thus seem to corroborate previous findings related to bismuth catalysts but contradict observations on tin catalysts. However, the increase in G_0 with temperature could also result from additional curing or from side reactions that lead to further crosslinking. Therefore, it cannot be considered definitive evidence of associative exchange, and additional experiments would be required to elucidate the mechanisms governing bond exchanges depending on the catalyst. Overall, a deeper understanding of TU reactions would be highly valuable for the design of PU CANs and for PU recycling.

Study of the recyclability of the materials

Thanks to their dynamic behaviour, the materials could be easily recycled by grinding and compression moulding (Fig. 6). FTIR was used to evaluate the main changes in the chemical structures of the networks after several reprocessing cycles (Fig. 7). Changes in the C=O stretching region were noticed after reprocessing for all the materials. The shape of the C=O in urethane bonds changes significantly, and new peaks at 1662 and 1625 cm^{-1}, which are characteristic of ureas, appear after reprocessing and tend to increase with further reprocessing cycles. This means that side reactions leading to urea formation happen during thermal reprocessing, regardless of the catalyst.

To evaluate the proportion of ureas formed during the reprocessing, deconvolution of the C=O stretching region was performed. The details of the deconvolution are given in the SI (Fig. S19–S22). The C=O region was accurately fitted with 6 gaussians, corresponding to different configurations of urethanes (free, ordered and disordered) and ureas (free, ordered and disordered), in good agreement with results

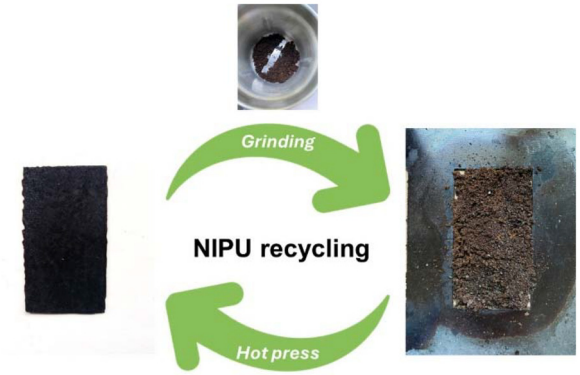

Fig. 6 Recycling of NIPU materials by grinding and compression moulding.

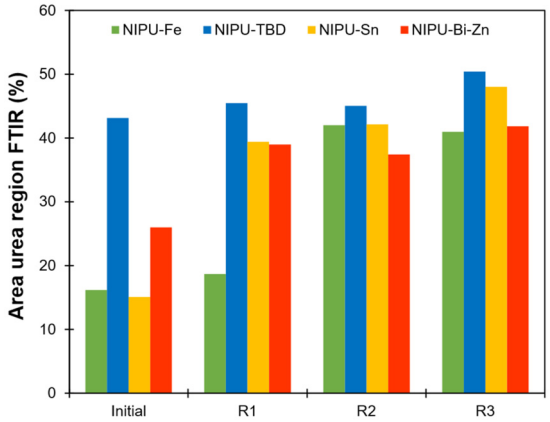

Fig. 8 Proportion of the C═O stretching band in FTIR related to ureas for the different NIPU materials after several reprocessing cycles.

recently reported by Jaques *et al.*[46] However, the lignin-based polyols already show significant absorption in the 1600–1800 cm^{-1} range (Fig. S23 in the SI), preventing a precise quantification of the ratio between ureas and urethanes. Therefore, we discuss here the area of the urea region in the FTIR spectra, keeping in mind that it may not truly represent the urea content because of the contribution of the lignin-based polyol.

Deconvolution confirms that **TBD** promotes the formation of ureas during NIPU synthesis, while **Fe**, **Sn** and to a lesser extent **Bi-Zn** can limit this phenomenon. However, the urea content rises after reprocessing, regardless of the catalyst (Fig. 8). The lowest urea contents are obtained with **Fe** and **Bi-Zn**, confirming their interest as TU catalysts for the synthesis of NIPUs. Ureas are often observed during NIPU synthesis by TU. They can form by the cross-metathesis of methyl carbamates, leading to the release of dimethyl carbonate (Scheme S3 in the SI).[80] However, the NIPU materials were syn-

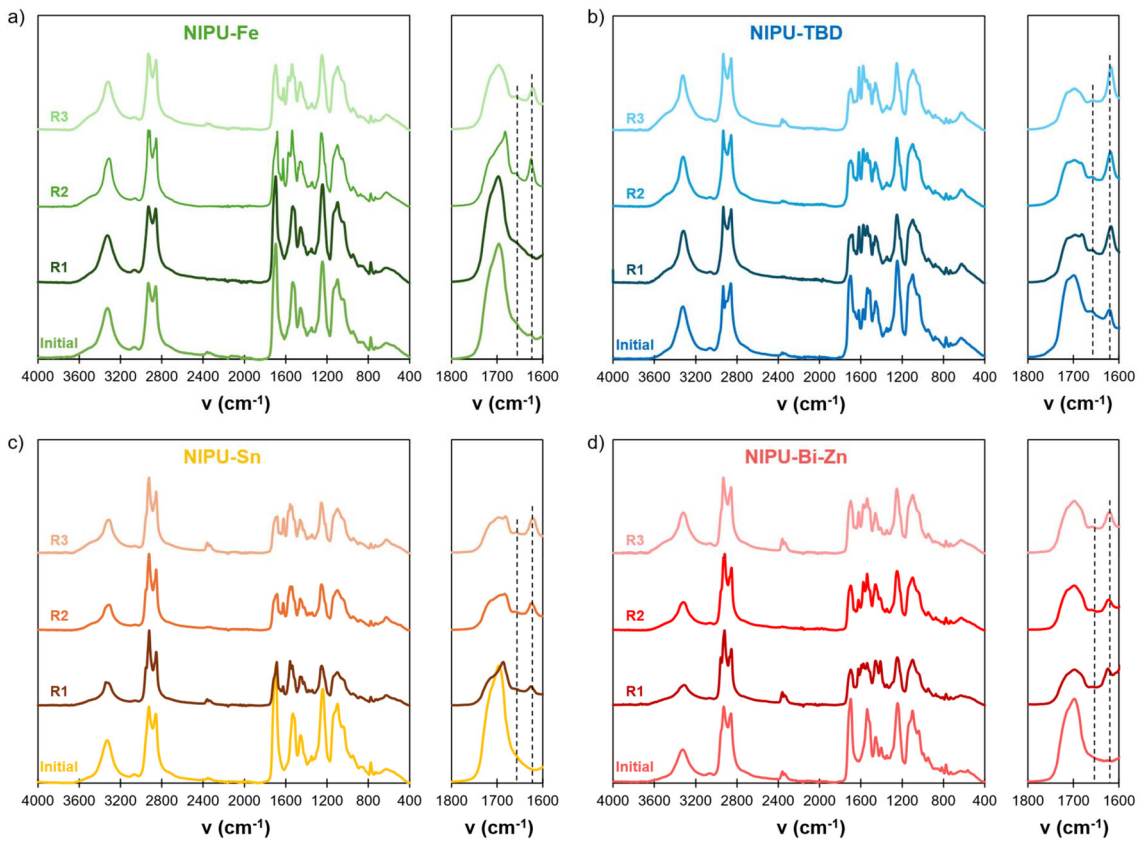

Fig. 7 FTIR spectra of the NIPU materials after several reprocessing cycles: (a) NIPU-Fe, (b) NIPU-TBD, (c) NIPU-Sn and (d) NIPU-Bi-Zn.

thesized with an excess of alcohol, meaning that most of the methyl carbamates have been consumed during the polymerization. The formation of ureas during reprocessing should then involve a different mechanism. The cross-metathesis mechanism described by Kébir *et al.*[80] could also involve non-terminal urethane groups, but it should lead to the formation of carbonate linkages within the polymer chains, in addition to the urea linkages. However, signals of carbonates are not seen on the FTIR spectra. As in our previous study, we noticed that water seemed to play a dramatic role in urea formation, which would point to a potential dissociative mechanism where isocyanates formed by dissociation of urethanes could react with residual water, forming amines and later urea linkages (Scheme S4 in the SI). The pronounced hydrophilic character of the materials, due to their high contents of PEG and KL, makes the mitigation of hygroscopicity a significant challenge, as the materials tend to absorb moisture despite rigorous drying protocols before the reprocessing cycles.

Except for **NIPU-Fe**, all the materials show a progressive decrease of T_g after reprocessing (Table 4 and Fig. S25 in the SI). A second relaxation around 120 °C is observed for all materials after reprocessing (Fig. S24 in the SI), even when it was absent on the virgin material, such as for **NIPU-Bi-Zn**. This means that the reprocessing tends to increase the phase separation between lignin-rich domains and a soft phase mostly consisting of PEG.

T_α measured by DMA follows the same decreasing trend as T_g after reprocessing (Table 4 and Fig. S25–S29 in the SI).

Table 4 Evolution of the thermal and mechanical properties of NIPU materials after several reprocessing cycles

Material	T_g (°C)	T_α (°C)	E (MPa)	σ (MPa)	ε (%)
NIPU-Fe	−14	18	7 ± 1	1.7 ± 0.2	28 ± 3
NIPU-Fe-R1	−13	21	8 ± 1	2.2 ± 0.4	43 ± 6
NIPU-Fe-R2	−13	10	29 ± 3	2.5 ± 0.2	29 ± 4
NIPU-Fe-R3	−15	13	41 ± 2	2.0 ± 0.4	14 ± 4
NIPU-TBD	−13	20	32 ± 2	4.5 ± 0.4	27 ± 4
NIPU-TBD-R1	−22	3	83 ± 2	5.5 ± 0.4	18 ± 3
NIPU-TBD-R2	−21	1	82 ± 14	4.4 ± 0.2	14 ± 1
NIPU-TBD-R3	−28	−4	97 ± 8	4.0 ± 0.2	9 ± 1
NIPU-Sn	−10	10	10 ± 1	1.0 ± 0.3	26 ± 8
NIPU-Sn-R1	−17	1	21 ± 1	1.3 ± 0.2	14 ± 2
NIPU-Sn-R2	−19	−6	49 ± 1	2.1 ± 0.1	11 ± 1
NIPU-Sn-R3	−23	−11	82 ± 2	2.9 ± 0.3	9 ± 2
NIPU-Bi-Zn	−6	19	10 ± 1	4.2 ± 0.3	72 ± 2
NIPU-Bi-Zn-R1	−8	17	15 ± 1	2.3 ± 0.3	35 ± 4
NIPU-Bi-Zn-R2	−9	9	23 ± 1	2.8 ± 0.4	35 ± 7
NIPU-Bi-Zn-R3	−14	8	38 ± 3	3.4 ± 0.2	28 ± 1

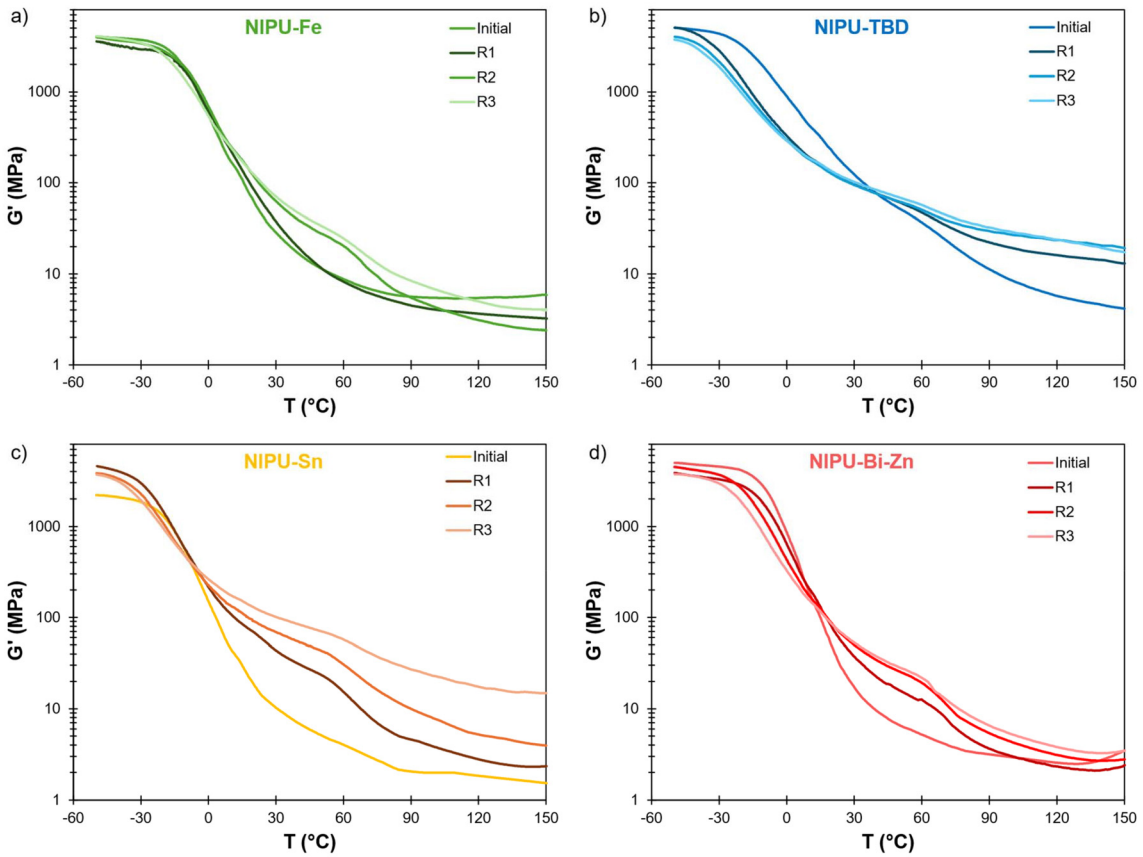

Fig. 9 Storage modulus G' measured by DMA of the NIPU materials after several reprocessing cycles: (a) NIPU-Fe, (b) NIPU-TBD, (c) NIPU-Sn and (d) NIPU-Bi-Zn.

Furthermore, all the materials show a significant increase in storage modulus G' after T_α, especially between 30 and 90 °C (Fig. 9). This is probably related to the observed increase in ureas, which contributes to enhancing the modulus by acting as physical crosslinks. Indeed, G' at 60 °C is well correlated to the area of the urea region measured by FTIR (Fig. S30 in the SI). For **NIPU-Fe** and **NIPU-Bi-Zn**, G' at high temperature ($T >$ 120 °C) remains in the same order of magnitude after reprocessing, indicating that the crosslink density is rather unchanged. On the other hand, it increases notably for **NIPU-TBD** and even more for **NIPU-Sn**. This means that additional crosslinking may have occurred, possibly by the formation of allophanates or biurets.[81–83] Allophanate formation is known to occur as a side reaction during PU synthesis, with basic[84] or tin catalysts.[85,86] However, the complexity of the FTIR spectra does not allow for the identification of allophanates,[87] and other analytical techniques should be deployed to gain further insights into their possible formation.[88]

Uniaxial tensile tests reveal that all the NIPU materials show rigidification after reprocessing, as shown by significant increases in Young's moduli (Table 4 and Fig. S31 and S32 in the SI). The elongations at break tend to decrease, probably because of increasing phase separation leading to structural heterogeneity. Interestingly, the Young's modulus of the NIPU materials is well correlated to the area of the urea region measured by FTIR (Fig. S30 in the SI), confirming that the increase in stiffness is mostly caused by the formation of rigid urea bonds.

Chemical recycling was also performed on **NIPU-Bi-Zn** (Scheme S5 in the SI). Unlike in our previous work, chemical recycling was successful without further addition of the catalyst.[47] The catalyst present in the material was sufficient to allow its complete depolymerization in methanol. After methanol evaporation, the depolymerized mixture was repolymerized as for the synthesis of the virgin material. As compared to the virgin material, the chemically recycled material has a lower T_g (−14 against −6 °C) and a more pronounced phase separation, revealed by the appearance of a second transition around 120 °C (Fig. S33 in the SI). FTIR shows the formation of ureas (Fig. S34 in the SI), which leads to an increase in the storage modulus measured by DMA (Fig. S33 in the SI), as already seen after thermomechanical recycling. Overall, the chemically recycled material is similar to the material after the first thermomechanical recycling cycle, offering another strong alternative for improving the end-of-life valorization of these lignin-based NIPUs.

Conclusion

This study demonstrates the successful synthesis of lignin-based NIPUs by TU, using a liquid polyol derived from KL and HMDC. In a preliminary approach, a model study allowed selecting 4 catalysts, which were then employed to synthesise NIPUs. By systematically evaluating the impact of the catalysts on NIPU properties and recyclability, we identified iron(III) acetylacetonate (**Fe**) and bismuth/zinc octanoate blend (**Bi-Zn**) as promising non-toxic alternatives to conventional tin-based catalysts or TBD. These catalysts not only promoted efficient TU reactions but also limited side reactions such as urea formation, which can compromise recyclability.

Upon adjustment of the stoichiometry between the reactants, NIPU networks containing free OH groups are easily obtained. This allows dynamic bond exchange leading to CAN behavior, as evidenced by stress relaxation experiments. Consequently, all materials could be successfully recycled three times by a simple thermomechanical process. However, changes in the chemical structure were identified, with the formation of urea linkages during reprocessing, leading to significant changes in the mechanical properties. However, **Fe** and **Bi-Zn** catalysts were able to limit this phenomenon and to avoid an increase in crosslink density during reprocessing, thus significantly improving the recyclability. Chemical recycling was also proven to be an alternative option for the end-of-life valorization.

In the context of the circular bioeconomy, this work clearly confirms that TU represents a powerful route for developing circular and biobased NIPUs, where the catalyst nature serves as a critical parameter for property optimization and recyclability. Subsequent investigations should elucidate the underlying exchange mechanisms—whether associative or dissociative—to better control network dynamics and minimize side reactions during the reprocessing steps.

Author contributions

Investigation: AR. Conceptualization and methodology: NW and AD. Formal analysis, data curation, and visualization: AR and AD. Resources, funding acquisition, and supervision: AD and LA. Writing – original draft: AD. Writing – review and editing: all.

Conflicts of interest

There are no conflicts of interest to declare.

Data availability

The data supporting this article have been included as part of the supplementary information (SI). Supplementary information is available. See DOI: https://doi.org/10.1039/d6py00044d.

Acknowledgements

We thank Agence Nationale de la Recherche (ANR, France) for financing the Biopoliol project (ANR-21-CE43-0026). We acknowledge the Cronenbourg NMR Core Facility (CNRS/

Université de Strasbourg, UMR 7042 LIMA, Strasbourg, France).

References

1 Plastics Europe, Plastics – the fast Facts 2024, https://plasticseurope.org/knowledge-hub/plastics-the-fast-facts-2024/, (accessed October 20, 2025).
2 P. Furtwengler and L. Avérous, *Polym. Chem.*, 2018, **9**, 4258–4287.
3 H. Sardon, D. Mecerreyes, A. Basterretxea, L. Avérous and C. Jehanno, *ACS Sustainable Chem. Eng.*, 2021, **9**, 10664–10677.
4 A. Delavarde, G. Savin, P. Derkenne, M. Boursier, R. Morales-Cerrada, B. Nottelet, J. Pinaud and S. Caillol, *Prog. Polym. Sci.*, 2024, **151**, 101805.
5 F. Souto and V. Calado, *Green Chem.*, 2022, **24**, 8172–8192.
6 D. D. S. Argyropoulos, C. Crestini, C. Dahlstrand, E. Furusjö, C. Gioia, K. Jedvert, G. Henriksson, C. Hulteberg, M. Lawoko, C. Pierrou, J. S. M. Samec, E. Subbotina, H. Wallmo and M. Wimby, *ChemSusChem*, 2023, **16**, e202300492.
7 A. Berlin and M. Balakshin, in *Bioenergy Research: Advances and Applications*, ed. V. K. Gupta, M. G. Tuohy, C. P. Kubicek, J. Saddler and F. Xu, Elsevier, Amsterdam, 2014, pp. 315–336.
8 L. Dessbesell, M. Paleologou, M. Leitch, R. Pulkki and C. (Charles) Xu, *Renewable Sustainable Energy Rev.*, 2020, **123**, 109768.
9 S. Mastrolitti, E. Borsella, A. Giuliano, M. T. Petrone, I. De Bari, R. Gosselink, G. van Erven, E. Annevelink, K. S. Triantafyllidis and H. Stichnothe, in *Sustainable lignin valorization - Technical lignin, processes and market development*, IEA Bioenergy, 2021.
10 A. Shafiq, I. Ahmad Bhatti, N. Amjed, M. Zeshan, A. Zaheer, A. Kamal, S. Naz and T. Rasheed, *Eur. Polym. J.*, 2024, **209**, 112899.
11 F. R. Vieira, S. Magina, D. V. Evtuguin and A. Barros-Timmons, *Materials*, 2022, **15**, 6182.
12 M. Alinejad, C. Henry, S. Nikafshar, A. Gondaliya, S. Bagheri, N. Chen, S. K. Singh, D. B. Hodge and M. Nejad, *Polymers*, 2019, **11**, 1202.
13 H. Li, Y. Liang, P. Li and C. He, *J. Bioresour. Bioprod.*, 2020, **5**, 163–179.
14 X. Ma, J. Chen, J. Zhu and N. Yan, *Macromol. Rapid Commun.*, 2021, **42**, 2000492.
15 J. Elms, P. N. Beckett, P. Griffin and A. D. Curran, *Toxicol. in Vitro*, 2001, **15**, 631–634.
16 H. Hamada, M. Bruze, E. Zimerson, M. Isaksson and M. Engfeldt, *Contact Dermatitis*, 2017, **77**, 231–241.
17 L. Maisonneuve, O. Lamarzelle, E. Rix, E. Grau and H. Cramail, *Chem. Rev.*, 2015, **115**, 12407–12439.
18 A. Gomez-Lopez, S. Panchireddy, B. Grignard, I. Calvo, C. Jerome, C. Detrembleur and H. Sardon, *ACS Sustainable Chem. Eng.*, 2021, **9**, 9541–9562.
19 M. Bourguignon, B. Grignard and C. Detrembleur, *Angew. Chem.*, 2022, **134**, e202213422.
20 M. Bourguignon, B. Grignard and C. Detrembleur, *J. Am. Chem. Soc.*, 2024, **146**, 988–1000.
21 T. Habets, B. Grignard and C. Detrembleur, *Prog. Polym. Sci.*, 2025, **165**, 101968.
22 N. Wybo, A. Duval and L. Avérous, *Angew. Chem., Int. Ed.*, 2024, **63**, e202403806.
23 N. Wybo, A. Duval and L. Avérous, *Mater. Today Sustain.*, 2025, **30**, 101117.
24 X. Meng, S. Zhang, B. Scheidemantle, Y. Wang, Y. Pu, C. E. Wyman, C. M. Cai and A. J. Ragauskas, *Ind. Crops Prod.*, 2022, **178**, 114579.
25 D. Li, B. Xue, Q. Zhao, W. Wang, X. Li, J. Wen, Z. Wang and W. Zhao, *Eur. Polym. J.*, 2024, **221**, 113553.
26 A. Salanti, L. Zoia, M. Mauri and M. Orlandi, *RSC Adv.*, 2017, **7**, 25054–25065.
27 J. Sternberg and S. Pilla, *Green Chem.*, 2020, **22**, 6922–6935.
28 J. Sternberg, O. Sequerth and S. Pilla, *Polymer*, 2025, **330**, 128516.
29 V. Mimini, H. Amer, H. Hettegger, M. Bacher, I. Gebauer, R. Bischof, K. Fackler, A. Potthast and T. Rosenau, *Holzforschung*, 2020, **74**, 203–211.
30 Y. Yang, H. Cao, R. Liu, Y. Wang, M. Zhu, C. Su, X. Lv, J. Zhao, P. Qin and D. Cai, *Ind. Crops Prod.*, 2023, **193**, 116213.
31 F. C. Destaso, C. Libretti, C. L. Coz, E. Grau, H. Cramail and M. A. R. Meier, *Green Chem.*, 2025, **27**, 1440–1450.
32 H. Hong, Z. Li, H. Wu, D. Wang, L. Liu, W. Luo, T. Yang, K. Yang and J. Yao, *Int. J. Biol. Macromol.*, 2025, **310**, 143259.
33 G. Rokicki and A. Piotrowska, *Polymer*, 2002, **43**, 2927–2935.
34 P. Deepa and M. Jayakannan, *J. Polym. Sci., Part A: Polym. Chem.*, 2008, **46**, 2445–2458.
35 M. Unverferth, O. Kreye, A. Prohammer and M. A. R. Meier, *Macromol. Rapid Commun.*, 2013, **34**, 1569–1574.
36 Y. Deng, S. Li, J. Zhao, Z. Zhang, J. Zhang and W. Yang, *RSC Adv.*, 2014, **4**, 43406–43414.
37 C. Duval, N. Kébir, A. Charvet, A. Martin and F. Burel, *J. Polym. Sci., Part A: Polym. Chem.*, 2015, **53**, 1351–1359.
38 N. Kébir, S. Nouigues, P. Moranne and F. Burel, *J. Appl. Polym. Sci.*, 2017, **134**, 44991.
39 S. Kotanen, P. Laurikainen, S. Lehtimäki, T. Harjunalanen, T. Laaksonen and E. Sarlin, *Int. J. Adhes. Adhes.*, 2024, **132**, 103726.
40 A. Martin, L. Lecamp, H. Labib, F. Aloui, N. Kébir and F. Burel, *Eur. Polym. J.*, 2016, **84**, 828–836.
41 P. Boisaubert, N. Kébir, A.-S. Schuller and F. Burel, *Polymer*, 2020, **206**, 122855.
42 P. Boisaubert, N. Kébir, A.-S. Schuller and F. Burel, *Eur. Polym. J.*, 2020, **138**, 109961.
43 P. Boisaubert, N. Kébir, A.-S. Schuller and F. Burel, *Polymer*, 2022, **240**, 124522.
44 V. Valette, N. Kébir, F. B. Tiavarison, F. Burel and L. Lecamp, *React. Funct. Polym.*, 2022, **181**, 105416.

45 N. G. Jaques, A. Llevot, É. Grau, T. Vidil, M. A. R. Meier and H. Cramail, *Macromol. Chem. Phys.*, 2025, **226**, 2500068.
46 N. G. Jaques, É. Grau, A. Llevot, T. Vidil, M. A. R. Meier and H. Cramail, *Macromol. Chem. Phys.*, 2025, **226**, e00207.
47 N. Wybo, E. Cherasse, A. Duval and L. Avérous, *J. Mater. Chem. A*, 2025, **13**, 11557–11572.
48 A. Duval, D. Vidal, A. Sarbu, W. René and L. Avérous, *Mater. Today Chem.*, 2022, **24**, 100793.
49 C. Bakkali-Hassani, D. Berne, P. Bron, L. Irusta, H. Sardon, V. Ladmiral and S. Caillol, *Polym. Chem.*, 2023, **14**, 3610–3620.
50 A. Basterretxea, E. Gabirondo, C. Jehanno, H. Zhu, I. Flores, A. J. Müller, A. Etxeberria, D. Mecerreyes, O. Coulembier and H. Sardon, *ACS Sustainable Chem. Eng.*, 2019, **7**, 4103–4111.
51 X. Meng, C. Crestini, H. Ben, N. Hao, Y. Pu, A. J. Ragauskas and D. S. Argyropoulos, *Nat. Protoc.*, 2019, **14**, 2627–2647.
52 N. Zheng, Z. Fang, W. Zou, Q. Zhao and T. Xie, *Angew. Chem., Int. Ed.*, 2016, **55**, 11421–11425.
53 P. Yan, W. Zhao, X. Fu, Z. Liu, W. Kong, C. Zhou and J. Lei, *RSC Adv.*, 2017, **7**, 26858–26866.
54 J. P. Brutman, D. J. Fortman, G. X. De Hoe, W. R. Dichtel and M. A. Hillmyer, *J. Phys. Chem. B*, 2019, **123**, 1432–1441.
55 D. J. Fortman, D. T. Sheppard and W. R. Dichtel, *Macromolecules*, 2019, **52**, 6330–6335.
56 D. T. Sheppard, K. Jin, L. S. Hamachi, W. Dean, D. J. Fortman, C. J. Ellison and W. R. Dichtel, *ACS Cent. Sci.*, 2020, **6**, 921–927.
57 M. Nath, *Appl. Organomet. Chem.*, 2008, **22**, 598–612.
58 B. Jousseaume, C. Laporte, T. Toupance and J.-M. Bernard, *Tetrahedron Lett.*, 2002, **43**, 6305–6307.
59 Y. Schellekens, B. V. Trimpont, P.-J. Goelen, K. Binnemans, M. Smet, M.-A. Persoons and D. D. Vos, *Green Chem.*, 2014, **16**, 4401–4407.
60 S. Kim, K. Li, A. Alsbaiee, J. P. Brutman and W. R. Dichtel, *Adv. Mater.*, 2023, **35**, 2305387.
61 M. Sun, D. T. Sheppard, J. P. Brutman, A. Alsbaiee and W. R. Dichtel, *Macromolecules*, 2023, **56**, 6978–6987.
62 B. Jousseaume, C. Laporte, T. Toupance and J. M. Bernard, *Tetrahedron Lett.*, 2003, **44**, 5983–5985.
63 L. Sougrati, A. Duval and L. Avérous, *ChemSusChem*, 2023, **16**, e202300792.
64 M. Brebu and C. Vasile, *Cellul. Chem. Technol.*, 2010, **44**, 353–363.
65 J. Sameni, S. Krigstin, D. dos Santos Rosa, A. Leao and M. Sain, *BioResources*, 2013, **9**, 725–737.
66 J. López-Beceiro, A. M. Díaz-Díaz, A. Álvarez-García, J. Tarrío-Saavedra, S. Naya and R. Artiaga, *Processes*, 2021, **9**, 1154.
67 S. Han, C. Kim and D. Kwon, *Polym. Degrad. Stab.*, 1995, **47**, 203–208.
68 S. Zhang, T. Liu, C. Hao, L. Wang, J. Han, H. Liu and J. Zhang, *Green Chem.*, 2018, **20**, 2995–3000.
69 A. Moreno, M. Morsali and M. H. Sipponen, *ACS Appl. Mater. Interfaces*, 2021, **13**, 57952–57961.
70 X. Ma, S. Li, F. Wang, J. Wu, Y. Chao, X. Chen, P. Chen, J. Zhu, N. Yan and J. Chen, *ChemSusChem*, 2023, **16**, e202202071.
71 A. Duval, W. Benali and L. Avérous, *Green Chem.*, 2024, **26**, 8414–8427.
72 L. Sougrati, A. Duval and L. Avérous, *Chem. Eng. J.*, 2025, **511**, 162201.
73 L. Sougrati, A. Duval and L. Avérous, *J. Mater. Chem. A*, 2025, **13**, 4921–4939.
74 A. Duval, W. Benali and L. Avérous, *ChemSusChem*, 2025, **18**, e202401480.
75 C. Bakkali-Hassani, D. Berne, V. Ladmiral and S. Caillol, *Macromolecules*, 2022, **55**, 7974–7991.
76 F. Elizalde, R. H. Aguirresarobe, A. Gonzalez and H. Sardon, *Polym. Chem.*, 2020, **11**, 5386–5396.
77 A. Breuillac, A. Kassalias and R. Nicolaÿ, *Macromolecules*, 2019, **52**, 7102–7113.
78 L. E. Porath and C. M. Evans, *Macromolecules*, 2021, **54**, 4782–4791.
79 B. Soman and C. M. Evans, *Soft Matter*, 2021, **17**, 3569–3577.
80 N. Kébir, M. Benoit and F. Burel, *Eur. Polym. J.*, 2018, **107**, 155–163.
81 A. Lapprand, F. Boisson, F. Delolme, F. Méchin and J.-P. Pascault, *Polym. Degrad. Stab.*, 2005, **90**, 363–373.
82 M. Gambiroža-jukić, Z. Gomzi and H. J. Mencer, *J. Appl. Polym. Sci.*, 1993, **47**, 513–519.
83 R. Van Maris, Y. Tamano, H. Yoshimura and K. M. Gay, *J. Cell. Plast.*, 2005, **41**, 305–322.
84 H. Ulrich, B. Tucker and A. A. R. Sayigh, *J. Org. Chem.*, 1967, **32**, 3938–3941.
85 K. Dusek, M. Spirkova and I. Havlicek, *Macromolecules*, 1990, **23**, 1774–1781.
86 T. Stern, *Polym. Adv. Technol.*, 2018, **29**, 746–757.
87 V. V. Zharkov and R. R. Vlasov, *J. Cell. Plast.*, 2022, **58**, 877–891.
88 A. Kumar and A. P. M. Kentgens, *Polymer*, 2025, **325**, 128245.